

Location of Organic Structure-Directing Agents in Zeolites Using Diffraction Techniques

Stef Smeets and Lynne B. McCusker

Abstract In this chapter, we delve into the X-ray diffraction techniques that can be used to address the question as to where the organic structure-directing agents (OSDAs) are located in the pores of a zeolite framework structure and give an overview of some of the practical issues involved. By examining the results of such investigations, we attempt to establish whether the OSDAs are really disordered, as is often claimed, or if it is the methods we use that give this impression. In fact, the non-framework species in the channels of a zeolite appear to be arranged quite logically in a chemically sensible manner. In most cases, the OSDA within the pores can be described well as a superposition of just a few discrete, symmetry-related positions, provided the discrepancies between the OSDA and framework symmetries can be resolved. On the basis of some selected examples, we show that their arrangements can be extracted from experimental data using a systematic strategy and sometimes supplementary information.

Keywords Simulated annealing • Structure-directing agents • X-ray (powder) diffraction • Zeolites

Contents

- 1 Introduction
- 2 Historical Perspective

S. Smeets (✉)
Department of Materials and Environmental Chemistry, Stockholm University, Stockholm
10691, Sweden
e-mail: stef.smeets@mmk.su.se

L.B. McCusker
Department of Materials, ETH Zurich, Zurich 8093, Switzerland

Department of Chemical Engineering, University of California, Santa Barbara, CA 93106,
USA

- 3 Brief Introduction to Powder Diffraction
 - 4 Locating the OSDA
 - 4.1 Rietveld Refinement
 - 4.2 Approximating the Scale Factor
 - 4.3 Generating and Interpreting a Difference Map
 - 4.4 Simulated Annealing
 - 4.5 Hydrogen in OSDAs
 - 4.6 R-values, Difference Plots, and Finalizing Matters
 - 5 Examples from Literature
 - 5.1 SSZ-87
 - 5.2 SSZ-61
 - 5.3 DAF-1
 - 5.4 SSZ-74
 - 5.5 RUB-50
 - 5.6 STA-2
 - 6 Discussion/Conclusion
- References

1 Introduction

Are the species in the pores of a zeolite framework structure really disordered as is often claimed? Or are they arranged logically in a chemically sensible manner and only appear to be disordered because of the methods we use to study them? If the latter is the case, can our methods be improved and/or supplemented to extract more correct information? In this chapter, we will attempt to answer these questions.

Even with the first syntheses of zeolites in the late 1940s, which sought to replicate the hydrothermal conditions that produced the natural zeolite minerals by heating mixtures of alkali and alkaline earth silicates and aluminates in sealed containers, structure analysis of the resulting product was considered to be of paramount importance. It was known that the negative charge of the aluminosilicate framework structure was balanced by the alkali and alkaline earth cations in the pores and that the pores were filled with water molecules, but why had one zeolite formed and not another? It was assumed that the answer would be revealed if the structure of the crystalline product could be determined.

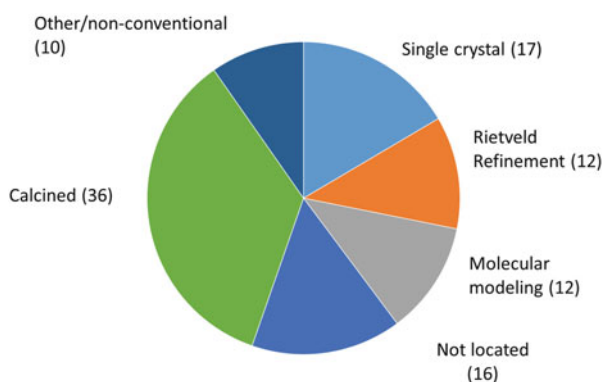
When Barrer and Denny included organic cations in the synthesis mixture in 1961, with the idea that by using a larger cation, the amount of Al in the framework could be reduced [1], it signalled the beginning of a new era in zeolite synthesis. Initially, simple tetramethylammonium (TMA) ions were used, but later on, as researchers began to realize that the organic cations also act as excellent structure-directing agents, increasingly complicated quaternary ammonium ions were tried. Now organic cations play a key role in most zeolite syntheses, and can have a profound effect on the micropore topology that results [2, 3]. Several groups have performed extensive systematic studies on the effect of the charge, shape, size, and composition of the organic cation on the end product [4–8].

Given the importance of these organic structure-directing agents (OSDAs) in modern zeolite synthesis, it is essential that we understand the interplay between the OSDA and the zeolite framework to understand why and how these materials form. It would be beneficial, therefore, if the locations of the organic guest species could be retrieved experimentally. Single-crystal X-ray diffraction (XRD) methods are ideal for this purpose, but most industrially and commercially important zeolites are only produced and used in polycrystalline form. Fortunately, powder diffraction methodology has now advanced to the stage where it is generally accepted that novel framework structures can be solved from X-ray powder diffraction (XRPD) data [9], and that inorganic cations in an as-synthesized or an ion-exchanged zeolite or zeolite-like material can be located with no problem. However, this is not yet the case for OSDAs. Locating a low-symmetry OSDA in the pores of a high-symmetry zeolite framework using XRPD data is fraught with difficulties.

To illustrate the scope of the problem, we catalogued the structures of the type materials of the 103 framework types that have been added to the Database of Zeolite Structures over the last 20 years [10]. We classified each material by how the OSDA was located (Fig. 1). In only 29 cases was the OSDA located experimentally, using either single-crystal or powder diffraction data. In 12 cases, the location of the OSDA was not determined from the data directly, but estimated instead using molecular dynamics modelling. In 16 cases, diffraction data on the as-made zeolite were available, but the researchers chose not to determine the location of the OSDA, or simply placed C atoms in the channels arbitrarily to describe the diffuse electron density cloud there without interpreting it further. In a small number of cases (10), the zeolite was synthesized in non-conventional ways, for example, in the absence of an OSDA [11], or using top-down methods [12, 13]. And in the remaining 36 cases, the structural characterization was performed on a calcined zeolite, where the problem of locating the OSDA is avoided.

The key difficulty in locating organic guest species in inorganic host structures from diffraction data is that organic compounds consist of light scatterers and typically have low point symmetry, while their inorganic hosts consist of heavier

Fig. 1 Pie chart showing the distribution of methods used to locate the SDA in the last 103 framework types (up to May 2017) published in the Database of Zeolite Structures [10]. In only 29 of the type materials reported was the OSDA located from the data directly, via either single-crystal methods or Rietveld refinement



scatterers and have high symmetry. These features result in a lack of contrast that makes it difficult to *see* the organic guest, and because of the difference in symmetry, the guest species often appear to be disordered. Even when decent quality single-crystal XRD data are available, these two factors alone make retrieving the location of the organic species challenging. The problem is exacerbated if the specimen is only available in polycrystalline form, when XRPD techniques are usually the only option. The process of locating the OSDA using XRPD data is often hindered by the quality of the data that can be collected. The problem may be low data resolution (no diffraction at higher angles and/or broad peaks), or in the assignment of reflection intensities when reflections overlap, a problem that is ubiquitous in powder diffraction. This adds a second layer of complication that often results in the guest species simply being dismissed as *disordered*. Perhaps for these reasons, the location of the OSDA in many studies is avoided, and structure analysis is performed using data collected on the calcined material. This is undesirable, because calcination typically leads to a reduction in the quality of the data that can be collected, and critical information related to the synthesis is lost.

Our own experience with as-synthesized zeolite structures indicates that the guest species actually tend to be highly ordered, and that their arrangements within the pores can often be described well as a superposition of just a few discrete, symmetry-related positions, provided the discrepancies between the OSDA and framework symmetries can be resolved. In this chapter, we will introduce the X-ray diffraction techniques used for locating OSDA molecules in zeolites, give an overview of some of the practical aspects of locating OSDAs, and highlight some examples of locating the OSDA.

2 Historical Perspective

As long as there have been synthetic zeolites, there have been researchers willing to take on the challenge of locating guest species in their pores, because their positions are considered to be essential to the understanding not only of the synthesis, but also of the properties of the resulting zeolite. For example, the synthesis [14] and crystal structure [15] of zeolite A, one of the first synthetic zeolites to be reported, were published in back-to-back papers in 1956. Its framework structure had no counterpart in the natural zeolites known at the time, and was deduced using chemical reasoning and powder diffraction data recorded on photographic film. With this information, 2-dimensional electron density maps were calculated in judiciously selected slices of the unit cell (calculations had to be done by hand as there were no computers), and even the positions of some of the sodium counterions could be resolved. Not only that, the positions of the counterions in several ion-exchanged forms of the zeolite were also determined. Somewhat later, when digitized single-crystal diffraction data and modest computing facilities were available, it was also recognized that the water molecules in the large cavity of zeolite A are not

randomly positioned as was first assumed, but arranged to form a hydrogen-bonded pentagon-dodecahedral cluster [16].

The conventional approach to locating the species in the pores of a known zeolite framework structure is to generate and interpret a 3-dimensional difference electron density (or Fourier) map. That is, the electron density calculated for the framework model is subtracted from the total electron density calculated from the measured reflection intensities to yield a map showing the residual density in the pores. See Sect. 4.3 for more details about how this is done in practice. These maps, while potentially extremely informative, are not always easy to interpret on the atomic level, especially if they have been generated from powder diffraction data. The interpretation is an iterative procedure that requires patience and perseverance on the part of the crystallographer and an understanding of the effects of the high symmetry of the framework on the lower symmetry OSDA. Nevertheless, the literature is full of examples of successful interpretations.

In the early studies of zeolites prepared with TMA in the synthesis mixture (late 1960s), only XRPD data could be obtained, but at least mainframe computers had become available and the cation was rigid and not too complicated. The difference Fourier approach described above was applied to TMA-sodalite, and the TMA cation was found to adopt an unexpected orientation in the sodalite cage with an unusually strong interaction between the cation and framework oxygen atoms [17]. The investigation of a second TMA zeolite was less straightforward. The presumed framework structure proved to be incorrect, so the authors considered how the four TMA cations per unit cell could be arranged, given the space group $I4_1/a$. The shape, size, and symmetry of the cation allowed only one arrangement. Then, by examining the distances between the TMA cations, it was possible to deduce where the aluminosilicate framework must be. In this way, the authors determined not only where the OSDAs were, but also that the framework structure was the same as that of the mineral gismondine [18].

The synthesis of ZSM-5 [19] was another milestone in the history of zeolite synthesis (1970s). Here, tetrapropylammonium (TPA) ions were used as the OSDA and it took years for the extremely complex high-silica framework structure to be deduced and reported [20, 21]. In a later publication, the approximate position of the TPA in the pores was found using single-crystal data from a very small crystal, but the geometry of the cation was severely distorted [22]. At this time, the Rietveld refinement technique for neutron powder diffraction data was being adapted to X-ray data, and powder diffraction methods began to evolve into a viable alternative for structure analysis. Using these new techniques and high-quality laboratory XRPD data, an improved description of the TPA could be obtained [23]. Finally, in 1987, large single crystals of ZSM-5 were produced and a definitive structure refined [24].

These early analyses of OSDAs in zeolitic materials were followed by many more, including those of zeolite-like aluminophosphates [25–27] and clathrasils [28–32] in the 1980s, and zincophosphates [33, 34] and gallophosphates [35–38] in the 1990s. Some were performed using single-crystal data and others using XRPD data. At this time, synchrotron radiation sources were beginning to become

accessible to research scientists, and this provided another boost to XRPD analysis. The high intensity and parallel nature of the synchrotron X-ray beam allowed extremely highly resolved XRPD patterns to be recorded. Such data were used to investigate the structure of the aluminophosphate VPI-5, which had been shown to have the largest channels known at the time [39]. A model for its framework structure had been proposed, but its fit to the measured neutron powder diffraction pattern was poor [40] and it was not clear how the simple linear dipropylammonium (DPA) cation that was used in the synthesis could produce such a large channel. In a careful analysis using synchrotron powder diffraction data collected on the as-synthesized form of VPI-5, it became apparent that the DPA cation had not been incorporated into the final structure at all, that some of the Al atoms in the framework were octahedrally coordinated, and that there was a well-ordered triple helix of hydrogen-bonded water molecules filling the 18-ring channel [41]. All this information was derived by hand from a series of difference Fourier maps. Each improvement to the model improved the quality of the electron density map and allowed one or two more atoms to be identified and eventually the mystery of the 18-ring channel to be resolved.

There are many more examples in the literature, and just a few representative studies have been referenced here. Generating and interpreting a difference map to locate non-framework species requires care and attention, and is sometimes described in great detail, especially when researchers were limited to X-ray powder diffraction data [42, 43]. This is in stark contrast to the studies where single-crystal X-ray data were available, where the result may be reduced to a single line, if mentioned at all. Certainly having single-crystal data helps, but such data do not guarantee an easily interpretable cloud of electron density in the pores of a zeolitic material. The problem of disorder produced by the high symmetry of the framework remains, even with the best data.

With modern computers, generating a difference electron density map is quick and easy, but the interpretation step is still time consuming. More recent studies take advantage of the ever-increasing computational power that is now available, and use molecular modelling and simulated annealing algorithms to obtain an initial location of the OSDA. This has allowed a more systematic approach to the problem to be developed.

3 Brief Introduction to Powder Diffraction

As most studies of zeolitic materials require the use of powder diffraction techniques, it is important to understand the basic principles involved. A powder diffraction pattern contains a lot of information, and some of the most important features are shown in Fig. 2. While some of these readily offer qualitative information about the material, extracting quantitative information requires somewhat more expertise (see Sect. 4.1).

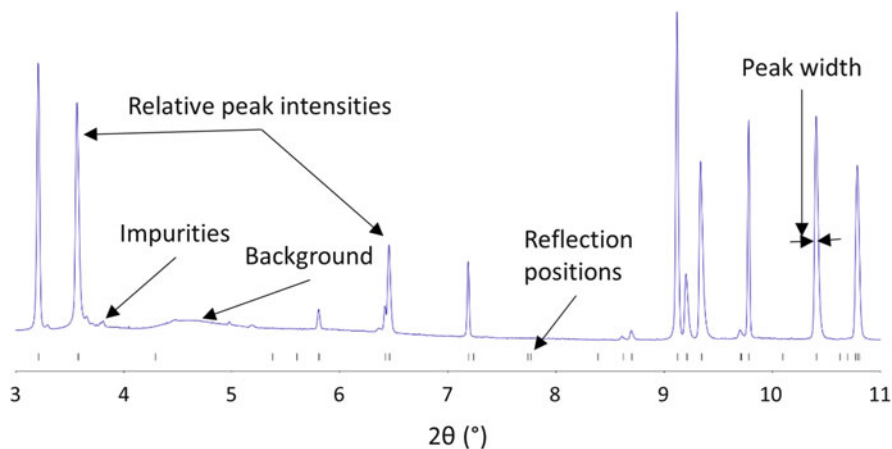


Fig. 2 A powder diffraction pattern, with the features of interest highlighted

In a powder diffraction pattern, the positions of the peaks (measured in $^{\circ}2\theta$) correspond to reflection positions. Note that a reflection does not necessarily give rise to a peak (the reflection may have an intensity of zero depending on the crystal structure), but a peak always indicates the presence of a reflection. The reflections correspond to the lattice spacings (also referred to as d -spacings) and therefore are determined solely by the size and shape of the unit cell of the crystalline phase. The unit cell is the smallest representative unit in the crystal lattice that can be translated in 3-dimensions to describe the bulk atomic arrangement of the material. Each peak corresponds to at least one reflection, and each reflection has a set of Miller indices (hkl) that are related to the unit cell. In a procedure called indexing, these hkl indices are assigned and the shape and size of the unit cell thereby determined. This is straightforward for materials with small unit cells and high symmetry, e.g. those with cubic or hexagonal crystal systems for which only one or two lattice parameters need to be determined, but is complicated by the fact that reflections that have similar d -spacings overlap. Overlapping reflections are undesirable, because they result in an ambiguity in the assignment of reflection intensities, which further complicates structure analysis. Crystalline phases with larger unit cells or lower crystallographic symmetry will typically generate more reflections and therefore more overlap. If all reflections can be indexed with a single unit cell, this is a good indication that the phase is pure. If there are reflections that are not indexed by the unit cell, this indicates that an additional crystalline phase is present or that the unit cell is incorrect. A large number of reliable auto-indexing programs are available for determining the unit cell from a list of peak positions (2θ values or d -spacings) [44].

If the positions of the reflections give information about the dimensions of the unit cell, then the relative reflection intensities describe the atomic decoration of the unit cell. In other words, the reflection intensities are related to the types and positions of the atoms (i.e. the electron density), and are the summation of all

X-ray photons diffracted by the crystals. The intensities are therefore related to the average crystal structure of the sample being studied. It is important to note that even a small change in the crystal structure (e.g. after ion exchange) will involve all reflection intensities, although some may be more affected than others.

Peak widths can be used as a first indicator of crystal quality. Narrow peaks mean small errors on the unit cell parameters, and are preferred for structural analysis, because overlapping reflections can be resolved more easily. They are dependent on the intrinsic instrumental peak width, stress or strain, and crystallite size (or, more precisely, size of the coherent domain). The smaller the crystallites, the broader the peaks become, especially for those smaller than 1 μm . For small plate-like or needle-shaped crystals, reflection broadening may occur along just one or two crystallographic directions (the short macroscopic dimensions), respectively, and this is referred to as anisotropic line broadening.

The background in a powder pattern corresponds to everything that cannot be described by the zeolite crystal structure. A high background can indicate the presence of a large amount of amorphous material (e.g. unreacted gel), but air scatter, the tail of the direct beam, or the glass capillary also contribute to the background. X-ray fluorescence from the sample may also occur and add to the background (e.g. if an Fe-containing material is measured using Cu $K\alpha$ radiation). The latter can be minimized by using a different wavelength.

4 Locating the OSDA

Typically, structural characterization of zeolites using diffraction data is split into two parts, (1) determining the framework structure, and (2) locating extra-framework species in the pores. Much attention has been devoted to the framework structure determination of zeolites using a wide array of techniques. For an up-to-date overview, the reader is referred to [9].

In the following sections, we assume that the framework structure is known, and focus on the problem of locating the OSDA (more generally referred to as structure completion). Structure completion is nearly always performed as an integral part of a Rietveld refinement, so we will first summarize the theory behind Rietveld refinement, paying particular attention to the problem of locating the OSDA and using modern computational tools (simulated annealing) to do so.

4.1 *Rietveld Refinement*

Rietveld refinement is named after a technique devised by Hugo Rietveld in 1969 to characterize crystalline materials using neutron powder diffraction data [45]. The method uses a least-squares approach to optimize a structural model until its powder pattern matches the measured one. At the time, it signalled a significant

advance in the structure analysis of powders, because it was able to deal with the problem of overlapping reflections in a reliable manner.

The theoretical intensity at step i , $Y(2\theta_i)$ can be defined as

$$Y(2\theta_i) = b(2\theta_i) + s \sum_h I_h G_h \phi(2\theta_i - 2\theta_h).$$

Here, I_h is the integrated diffracted intensity of the h th reflection, G_h is a function that corrects for preferred orientation, ϕ is the normalized profile function describing the shape of the reflections (e.g. the half-width, or peak asymmetry), b is the background function that describes the background at $2\theta_i$, and s is a scale factor. The intensities of the reflections depend on many factors, and for a more detailed description the reader is referred to a dedicated textbook such as *The Fundamentals of Crystallography* [46]. In general, it holds that the diffracted intensity is proportional to the structure factor multiplied by its complex conjugate:

$$I_h \propto F_h F_h^* = |F_h|^2.$$

Structure factors are calculated from the atomic parameters of the model using the equation

$$F_h = \sum_j n_j f_j \exp \left[2\pi i (hx_j + ky_j + lz_j) \right],$$

where F_h is the sum over all atoms in the unit cell. x_j , y_j , and z_j are the fractional coordinates, n_j is the population parameter (also referred to as the occupancy), and f_j the atomic form factor describing the shape of the observed atomic electron density of the j th atom.

In practice, Rietveld refinement can be broken down into the following steps:

1. Collection of the powder diffraction data.
2. Determination of the background function.
3. Determination of the peak shape function.
4. Evaluation of the starting values for the profile parameters.
5. Selection of the space group.
6. Refinement of the unit cell and profile parameters.
7. Addition of a (partial) structural model with geometric restraints.
8. Scaling of the calculated pattern to the observed data.
9. Structure completion.
 - (a) Generation of a difference electron density map.
 - (b) Interpretation of the difference electron density map.
 - (c) Repetition of steps a and b until the structural model is complete.
10. Rietveld refinement of the structural and profile parameters.

Note that Rietveld refinement is initiated only in step 10, and that each of the steps preceding the Rietveld refinement is concerned with estimating the initial parameters as well as possible. This includes the crystal structure, which should be approximately correct and complete. If it is not, Rietveld refinement will simply not converge sensibly. Once the refinement is underway, there are several numerical criteria of fit that can be used to evaluate the state of the refinement, and to judge the quality of the fit. The most commonly reported one is the (weighted) profile agreement value

$$R_{wp} = \left[\frac{\sum_i w_i (Y_i^{\text{obs}} - Y_i^{\text{calc}})^2}{\sum_i w_i (Y_i^{\text{obs}})^2} \right]^{0.5}$$

Here, Y_i^{obs} and Y_i^{calc} are the observed and calculated profile intensities at data point i , and w_i is the weight given to each data point, conventionally taken as $w_i = 1/Y_i^{\text{obs}}$.

These steps have not changed much over the last 30 years, and are dealt with in detail in other publications. In particular for points 1–7, readers are referred to the *Rietveld refinement guidelines* [47] and *The Rietveld Method* [48]. Although only step 10 is directly related to the problem of locating the OSDA, the other steps have an important effect on the quality of the outcome. Programs that are widely used for Rietveld refinement include TOPAS [49], GSAS [50], and Fullprof [51].

The peak shape and other profile or instrument parameters are best determined beforehand, as part of a model-free whole profile fit [52, 53]. These parameters can then be kept fixed until the final stages of the Rietveld refinement. In our experience, this improves the stability of the refinement with a partial model. Background correction can also be performed as part of the model-free whole profile fit. Manual removal of the background is preferred, because of the added control it gives over the sometimes erratic and unreliable nature of fitting a polynomial, especially when the structural model is incomplete.

Rietveld refinement of zeolites is usually initiated after a geometric optimization of the framework. A program like TOPAS [49] offers the possibility of performing a geometrical refinement against the angle and distance restraints using the “penalties_only” instruction. Another option is to use a dedicated distance-least-squares algorithm as implemented in the program DLS-76 [54], or a molecular modelling program like GULP [55]. This ensures that the refinement is started with a sensible framework geometry.

4.2 Approximating the Scale Factor

One of the first tasks after the zeolite model has been introduced and profile parameters determined is to scale the calculated pattern so that it matches the observed one. This is a trivial task when the initial structural model closely matches

the true one, but is complicated for as-synthesized zeolites if the position of the OSDA has not yet been accounted for. The presence or absence of non-framework species has a noticeable effect on the relative intensities in the low-angle region. A calcined material typically has much higher relative peak intensities in the low-angle region than does the as-synthesized material. The high-angle region is usually less sensitive to the presence of electron density in the zeolite channels, and more affected by small deviations in the positions in the atoms in the framework, atomic displacement (thermal vibrations of the atoms), defects, bond lengths, and the presence of heteroatoms. Figure 3 shows the powder patterns calculated for zeolite SSZ-87 with and without the OSDA included.

This gives a little bit of a chicken-and-egg problem for zeolites, because to determine the scale factor accurately, the position of the OSDA should be known, but to determine the position of the OSDA, the scale factor should be as accurate as possible. To get around this, the scale factor (for the whole pattern) is usually determined using only the high-angle data, which are less sensitive to the position of non-framework species. A reasonable estimate of the scale factor can be made by performing a few cycles of refinement with all other parameters fixed. If the profile

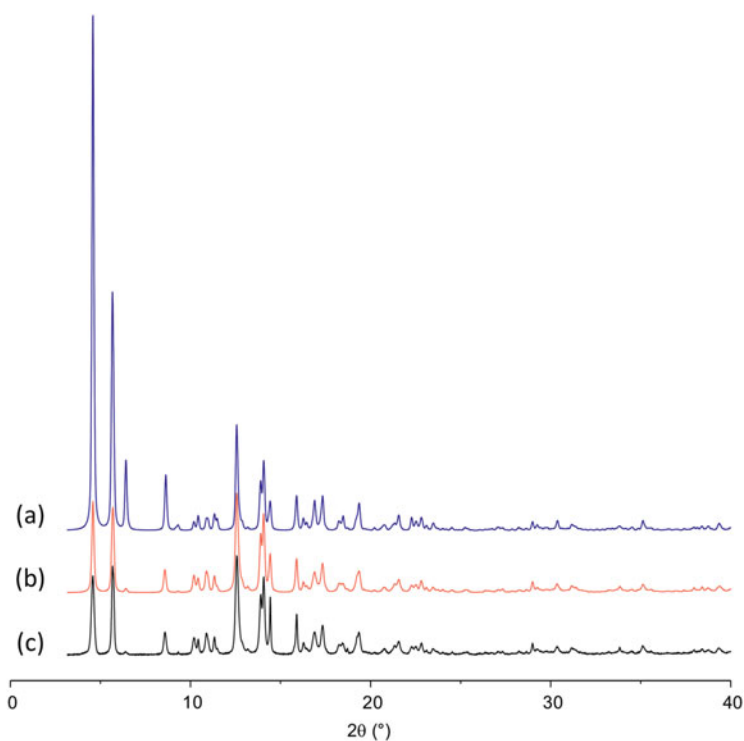


Fig. 3 Powder diffraction pattern of SSZ-87 (a) calculated using the framework atoms only, (b) calculated using the framework atoms and the OSDA, and (c) the observed data

fit at the higher 2θ angles is not good, the background probably needs to be adjusted. In most cases, this gives a good first approximation of the scale factor.

4.3 *Generating and Interpreting a Difference Map*

To get a low-resolution estimate of the location of the OSDA, a difference Fourier map, sometimes also referred to as simply a difference map or residual electron density map, is generated. These maps can be generated by subtracting the electron density map corresponding to the structural model from that calculated using the “observed” intensities. The word “observed” here is in quotation marks, because the observed intensities are actually extracted by assuming that the ratios of the reflection intensities in an overlap group calculated using the incomplete structural model are the same for the full structure. Although this usually gives a good approximation, it is important to keep in mind that the Fourier difference map is always biased towards the model used to calculate it.

A difference Fourier map thus highlights the structural difference between the observed and calculated data, and should reveal any residual electron density that has not been accounted for by the model. The algorithms needed to generate difference Fourier maps are standard in most suites of crystallographic programs, and can be visualized in programs like VESTA [56] or Chimera [57], if such functionality is not available within the Rietveld refinement program itself.

Figure 4a shows an example of a high-quality difference map obtained during a refinement of as-synthesized ZSM-5. It is trivial to recognize the shape of the TPA ion, even though there is some minor disorder in the “arms” of the cation. Figure 4b shows a more typical difference map, which corresponds to the difference between

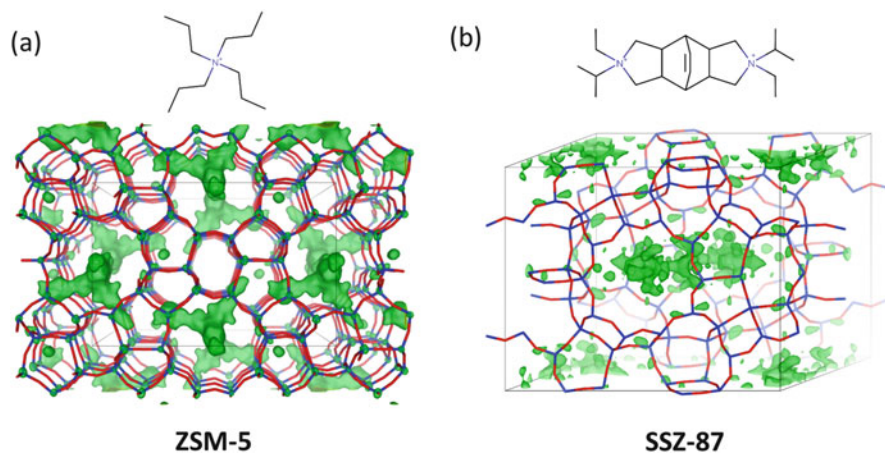


Fig. 4 Example of (a) a high-quality difference map for ZSM-5, and (b) a normal-quality difference map for SSZ-87. The corresponding OSDAs are shown above the difference maps

the observed and calculated patterns shown for as-synthesized SSZ-87 in Fig. 3. Although it is clear that the residual density describes the rough shape of the OSDA, its actual orientation cannot be discerned.

As noted above, most of the information about the residual electron density in the channel system is in the low-angle portion of the powder diffraction pattern. For the best results, it is therefore important that the scale factor be accurate, and determined using the high-angle data only. If the whole pattern is used to determine the scale factor, the differences will be too low at low angles, and too high at high angles. Figure 5 shows an example for as-synthesized ZSM-5 where the scale factor has been determined in this way. Here, the scale factor is too low by a factor of two, which results in significant electron density located on the framework atoms, and the shape of the OSDA can no longer be made out from the sliver of electron density that remains.

The crux of the problem in locating the OSDA lies in the interpretation of the electron density map. Non-framework species rarely follow the (usually higher) symmetry of their hosts. For example, an atom that is near a mirror plane of the framework (but not on it) will always be accompanied by a mirrored copy of itself on the other side (Fig. 6a). That is, it occupies two positions that are equivalent by

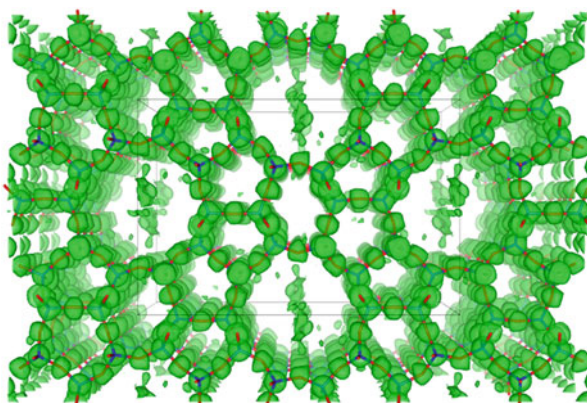


Fig. 5 Example of a difference map for ZSM-5, where the scale factor is refined against the entire diffraction pattern

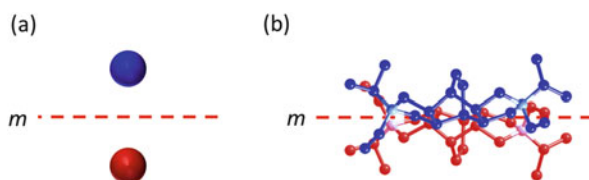


Fig. 6 Example of an (a) atom near a mirror plane, and (b) the OSDA used to synthesize SSZ-87 near a mirror plane. The equivalent species are coloured red and blue to distinguish them. In both cases, the maximum occupancy is 0.5

symmetry. Because the two positions are too close to be populated at the same time, the maximum occupancy of this position is 0.5. Interpretation of an electron density map corresponding to such a situation is manageable in simple cases, such as a Na^+ ion or a water molecule, but is much more difficult for a complicated OSDA, especially as positions of fourfold symmetry or higher are not uncommon (Fig. 6b). This problem of partial occupancy, or disorder of the OSDA, is common for zeolites, and greatly hampers the interpretation of the difference map. With powder diffraction data, the problem is exacerbated, because the observed reflection intensities are only approximated, and this causes the map to be somewhat more diffuse.

Even with high-quality single-crystal XRD data, individual atoms can rarely be discerned. Although the better intensities alleviate some of the problems related to generating and interpreting a difference map, they do not solve the disorder problem and it is rare that individual atoms can be seen when a symmetry element is nearby. With powder diffraction data, of course, the effect is even more pronounced.

4.4 *Simulated Annealing*

As part of our own research, we have found the simulated annealing (SA) routine to be very effective in locating organic guest species in zeolites from XRPD data [58]. SA has gained most attention in the area of crystallography as the method of choice for determining organic structures from powder diffraction data [59], but it is flexible enough to deal with various types of other materials also. Indeed, it was used initially as a method for determining zeolite framework structures from powder data [60], and has since been used to locate adsorbed species in zeolites [61–64], the OSDA in germanates [65, 66] and the organic linkers in MOFs [67–69]. Simulated annealing is a global optimization algorithm that is used in a wide variety of computational problems. In the context of crystal structure determination, it belongs to the direct-space class of methods [59]. Direct-space methods were introduced almost 30 years ago, but have been significantly facilitated by the increase in computational power that has become available over the last 20 years. They have now matured to a degree where they are widely implemented in Rietveld refinement suites like TOPAS [49], GSAS [50], and Fullprof [51], or dedicated programs like FOX [70] or DASH [71]. The idea behind direct-space methods is conceptually simple and effective when some prior information about the system, such as the chemical composition, geometry, or connectivity, is known.

Expected atoms, molecules, or fragments are defined as rigid bodies, and placed in the unit cell in a random arrangement. During an iterative procedure, their positions, orientations, and any free torsion angles are modified. After each rearrangement, the corresponding diffraction pattern is calculated and compared with the observed one. If the fit is better than the previous one, the move is accepted; if it is worse, the decision as to whether or not to accept the move is

made by a simulated annealing algorithm (accepting more “false” moves initially and fewer as the procedure progresses). After convergence has been reached (based on R_{wp} or some other criterion), the process is repeated until a satisfactory model that fits the data emerges.

Direct-space methods are widely applied for structure determination of pharmaceutical and organic compounds, for which the molecular connectivities are usually known. This also makes them ideally suited for tackling the problem of locating organic guests in inorganic host materials, for which the chemical composition and connectivity are usually known, and can be confirmed using elemental analysis and solid state $[13]C$ NMR, respectively. Because the algorithm uses the experimental diffraction pattern directly, the data quality is reflected in the profile parameters used to calculate the pattern for each model generated, so the problem of reflection overlap is circumvented. Furthermore, complicated partial occupancies arising from the OSDA being near or on a high-symmetry site are taken into account automatically.

Simulated annealing therefore offers a straightforward way of interpreting the inevitably low-resolution electron density clouds representing the OSDA in a difference Fourier map in an objective manner. There are several ways of introducing the OSDA molecule as a rigid-body model into the structural model. If the structure of the OSDA has been determined before, online databases such as the Cambridge structural database [72] are obvious sources for obtaining a model of the OSDA. An approximate model can also be generated from scratch, and optimized using molecular modelling programs like Avogadro [73] or Jmol [74]. These allow a three-dimensional model of the OSDA to be constructed interactively or via the SMILES syntax [75]. How the model of the OSDA should be introduced into the Rietveld refinement, depends on the program used. FOX, DASH, Fullprof, GSAS, and TOPAS all expect the rigid-body to be in the Fenske-Hall Z-matrix format, or a modified version thereof. An example of the Z-matrix format used by TOPAS is given for TPA in Fig. 7. The program Babel [76] is useful for handling some of the necessary coordinate transformations.

A rigid-body model has three rotational and three translational parameters associated with it. Additional internal rotations of rigid subgroups may also be

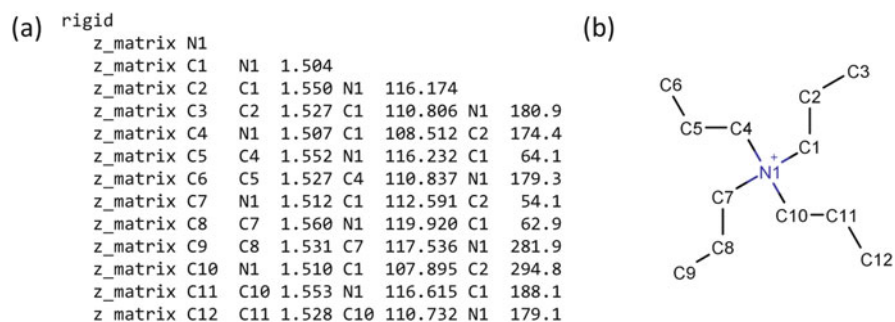


Fig. 7 (a) Example of a Z-matrix in TOPAS, corresponding to (b) tetrapropylammonium (TPA)

introduced, at the cost of more degrees of freedom. After the OSDA is introduced into the model, the global optimization can be initiated. During the optimization process, all parameters, except the six parameters describing the location and orientation of the OSDA, should remain fixed. The occupancy of the OSDA can usually be estimated from the location of the electron density cloud in the difference map, but sometimes allowing the global optimization to find a good value is helpful. Sometimes it is worthwhile to allow the scale factor to refine as well, because it can influence the fitting of the OSDA.

In our experience with TOPAS, we have not found it necessary to deviate from the default settings. Because the problem of locating the OSDA is usually well defined, the simulated annealing procedure takes no longer than a few minutes to determine a reliable starting position for further refinement. If it does not find a solution in that time, it is usually not worth continuing for a longer period. Time is better spent by changing the strategy. For example, the occupancy of the OSDA can be allowed to refine, the background and/or scale factor can be re-estimated, or “anti-bump” restraints can be introduced. If necessary, H atoms can be modelled by scaling the occupancy of the parent atom to account for the additional electron density (see Sect. 4.5). Once a suitable location for the OSDA has been found, the rigid-body parameters can also be refined further. Usually we keep the rigid-body model to refine the position of the OSDA for a couple of cycles of Rietveld refinement, and only after the refinement has converged sufficiently, do we exchange the rigid-body model for a restrained one (e.g. using the tabulated distances and angles in the International Tables for Crystallography, Vol. C, Chapter 9.5 [77] as a guide).

It is useful to know the convention the program uses to relate the rigid-body model to its placement in the unit cell, and how to take advantage of this. For example, for a rigid-body in the program TOPAS, the first atom in the Z-matrix is taken as the centre of the molecule. The second atom defines the z -axis, and the third atom the xz -plane. The x -axis is in the same direction as the a lattice vector, and y is in the ab -plane. By choosing the first three atoms carefully, the placement of the molecule can sometimes be directed by aligning it with a symmetry element. In some cases, a “dummy” atom with occupancy equal to zero is needed to achieve this. In doing so, some of the translations and/or rotations can be fixed, and the search space for the position of the OSDA reduced considerably. Note that the maximum occupancy of the OSDA should be reduced accordingly.

4.5 *Hydrogen in OSDAs*

XRPD data are not very sensitive to the position of hydrogen atoms as they only contribute one electron and that is delocalized in bonding. However, the contribution of a large number of hydrogen atoms adds up, and can make a small, but noticeable contribution to the observed reflection intensities. For OSDAs, hydrogen can easily contribute up to 30% of the electron density, and therefore needs to be

accounted for in one way or another. Some programs allow H atoms to be added in the geometrically expected positions. Otherwise, the population of the parent atom can be inflated to account for the additional electron density. For example, the electron count of a $-\text{CH}_3$ group can be modelled by omitting the H atoms, but inflating the population of the C atom by a factor of 1.5 to account for the nine electrons in $-\text{CH}_3$.

4.6 *R-values, Difference Plots, and Finalizing Matters*

The progress of the Rietveld refinement is usually monitored by following the trend in the agreement values (i.e. R_{wp}). Unfortunately, there are no absolute thresholds for these agreement values that signal that a refinement is finished. It is important to keep in mind that the value of R_{wp} , while internally consistent, merely represents the quality of the fit of the model to the data. Therefore, it says absolutely nothing about the quality of the structure.

Therefore, criteria of fit only tell part of the story, and other criteria are equally, if not more, important. A visual representation of the fit of Y^{calc} to Y^{obs} along with a plot of the differences ($Y^{\text{obs}} - Y^{\text{calc}}$) can reveal problems with the profile parameters, such as peak shape, background, zero correction, sample displacement, and unit cell. The physical meaning of mismatches in intensities is best visualized by calculating a difference electron density map. A difference map can uncover problems with the structure, the position of the OSDA, or with the symmetry, but it is important to remember that the difference map is biased towards the model. Positive residual electron density peaks can indicate missing atoms, while negative peaks may indicate atoms that are only partially occupied or absent. A good indication of the quality of the refinement is how clean the residual density map is (i.e. the map is featureless).

Finally, all of this is in vain if the refined structure does not make chemical sense. It is necessary to monitor the bond angles and distances, intramolecular distances, occupancies, and atomic displacement parameters during the course of the refinement to verify that they correspond to reasonable values.

1. *Is the geometry of the framework reasonable?* For high-silica zeolites, the criteria we use are as follows:

$$\begin{aligned} 1.55 \text{ \AA} &\leq d(\text{Si} - \text{O}) \leq 1.65 \text{ \AA} \\ 104.0^\circ &\leq \sphericalangle(\text{O} - \text{Si} - \text{O}) \leq 114.0^\circ \\ \sphericalangle(\text{Si} - \text{O} - \text{Si}) &\geq 135.0^\circ \end{aligned}$$

2. *Are the intermolecular distances between the framework and any non-framework species reasonable?* For example, for the OSDA, we try to

maintain a framework-to-OSDA distance of at least 3.0 Å unless there is a chemical bond involved.

3. *Are the interatomic distances within the OSDA sensible?* In a restrained refinement these do not usually deviate much from the expected values (i.e. ± 0.02 Å).
4. *Are the atomic displacement parameters sensible?* As a rule of thumb, the B_{iso} values we use are for Si: 1.0–2.0, for O: 2.0–3.0, and for the OSDA or extra-framework water: 3.0–5.0.
5. *Are the occupancies sensible?* For example, the occupancy of an OSDA on a position of fourfold symmetry can never exceed 0.25, or the population sum of two atoms occupying the same site (like Ge and Si in a germanosilicate) has to equal one.

Only if all qualitative criteria are fulfilled, and quantitative criteria are stable and as low as possible, can the refinement be considered finished.

5 Examples from Literature

It is clear that locating the OSDA from XRPD data requires a great deal of care and attention in all but the most trivial cases. Perhaps for this reason, the process of locating the OSDA is sometimes described in great detail. This section is intended to highlight a few of those studies where the location of the OSDA from diffraction data is central.

Table 1 shows a summary of studies in which the OSDA has been located over the last 20 years, and includes the 29 cases from the Database of Zeolite Structures mentioned in the introduction, as well as some selected recent studies.

5.1 SSZ-87

Cell: $C2/m$, $a = 21.1727$ Å, $b = 17.8092$ Å, $c = 12.2869$ Å, $\beta = 124.79^\circ$

Composition: $[(C_{22}H_{42}N_2)_2][Si_{64}O_{128}]$

The borosilicate SSZ-87 (**IFW**) was found as a product in a new synthesis approach for silica-based zeolites using boric acid and ammonium fluoride [78]. The framework structure of SSZ-87 was determined using electron diffraction data, and revealed a framework with large cages interconnected by 8- and 10-ring channels, giving rise to a three-dimensional channel system. After the geometry of the framework had been optimized, the scale factor was estimated and a difference map generated using the method described in Sect. 4.3. Most of the residual electron density is located in the large $[10^28^46^85^84^8]$ cavity (Fig. 4b). Although the electron density cloud has the rough shape of the OSDA, its actual orientation is difficult to discern, presumably because of the high degree of reflection overlap (93%) and the

Table 1 List of some zeolites in which the location of the OSDA has been determined using diffraction techniques

Material	Code	Year	Data	Reference	Method ^a
<i>SSZ-23</i>	STT	1998	Single-crystal XRD	[88]	DiffMap
<i>UCSB-15GaGe</i>	BOF	1998	Single-crystal XRD	[89]	DiffMap
<i>UCSB-7</i>	BSV	1998	Single-crystal XRD	[89]	DiffMap
<i>UCSB-9</i>	SBN	1998	Single-crystal XRD	[90]	DiffMap
<i>Mu-18</i>	UEI	2001	Single-crystal XRD	[91]	DiffMap
<i>UiO-28</i>	OWE	2001	Single-crystal XRD	[92]	DiffMap
<i>RUB-10</i>	RUT	2001	Powder XRD	[93]	DiffMap
<i>AIPO-SAS</i>	SAS	2002	Single-crystal XRD	[94]	DiffMap
<i>AIPO-CHA</i>	CHA	2002	Single-crystal XRD	[94]	DiffMap
<i>IST-1</i>	PON	2003	Powder XRD	[95]	DiffMap
<i>ITQ-12</i>	ITW	2004	Powder XRD	[96]	DiffMap
<i>Nu-6</i>	NSI	2004	Powder XRD	[97]	DiffMap
<i>SU-16</i>	SOS	2005	Single-crystal XRD	[98]	DiffMap
<i>SIZ-10</i>	CHA	2006	Single-crystal XRD	[99]	DiffMap
<i>SU-15</i>	SOF	2008	Single-crystal XRD	[100]	DiffMap
<i>SU-32</i>	STW	2008	Single-crystal XRD	[100]	DiffMap
<i>SSZ-74</i>	-SVR	2008	Powder XRD	[80]	Modelling
<i>PKU-9</i>	PUN	2009	Single-crystal XRD	[101]	DiffMap
<i>LSJ-10</i>	JOZ	2010	Single-crystal XRD	[102]	DiffMap
<i>RUB-50</i>	LEV	2010	Powder XRD	[82]	MEM
<i>STA-2</i>	SAT	2010	Powder XRD	[86]	Modelling
<i>Linde type J</i>	LTJ	2011	Powder XRD	[103]	DiffMap
<i>CoAPO-CJ69</i>	JSN	2012	Single-crystal XRD	[104]	DiffMap
<i>CoAPO-CJ62</i>	JSW	2012	Single-crystal XRD	[105]	DiffMap
<i>SSZ-52</i>	SFW	2013	Powder XRD	[106]	Modelling
<i>JU-92-300</i>	JNT	2013	Single-crystal XRD	[107]	DiffMap
<i>ZnAlPO-57</i>	AFV	2014	Powder XRD	[108]	DiffMap
<i>ZnAlPO-59</i>	AVL	2014	Powder XRD	[108]	DiffMap
<i>SSZ-45</i>	EEI	2014	Powder XRD	[109]	SAnnealing
<i>SSZ-61</i>	*-SSO	2014	Powder XRD	[79]	SAnnealing
<i>EMM-23</i>	*-EWT	2014	Powder XRD	[110]	Modelling
<i>SSZ-87</i>	IFW	2015	Powder XRD	[78]	SAnnealing
<i>Ge-BEC</i>	BEC	2015	Powder XRD	[111]	SAnnealing
<i>DAF-1</i>	DFO	2015	Powder XRD	[43]	DiffMap
<i>ITQ-24</i>	IWR	2015	Powder XRD	[42]	DiffMap
<i>EU-12</i>	ETL	2016	Powder XRD	[112]	Not reported
<i>SSZ-53</i>	SFH	2016	Powder XRD	[58]	SAnnealing
<i>SSZ-55</i>	ATS	2016	Powder XRD	[58]	SAnnealing
<i>SSZ-56</i>	SFS	2016	Powder XRD	[58]	SAnnealing
<i>SSZ-58</i>	SFG	2016	Powder XRD	[58]	SAnnealing
<i>SSZ-59</i>	SFN	2016	Powder XRD	[58]	SAnnealing
<i>CIT-13</i>	–	2016	Powder XRD	[113]	SAnnealing

(continued)

Table 1 (continued)

Material	Code	Year	Data	Reference	Method ^a
<i>EMM-26</i>	–	2016	Powder XRD	[114]	DiffMap
<i>ITQ-37</i>	-ITV	2016	Single-crystal XRD	[115]	DiffMap

^a*DiffMap* interpretation of the difference map, *SAnnealing* simulated annealing, *Modelling* molecular modelling, *MEM* maximum entropy method

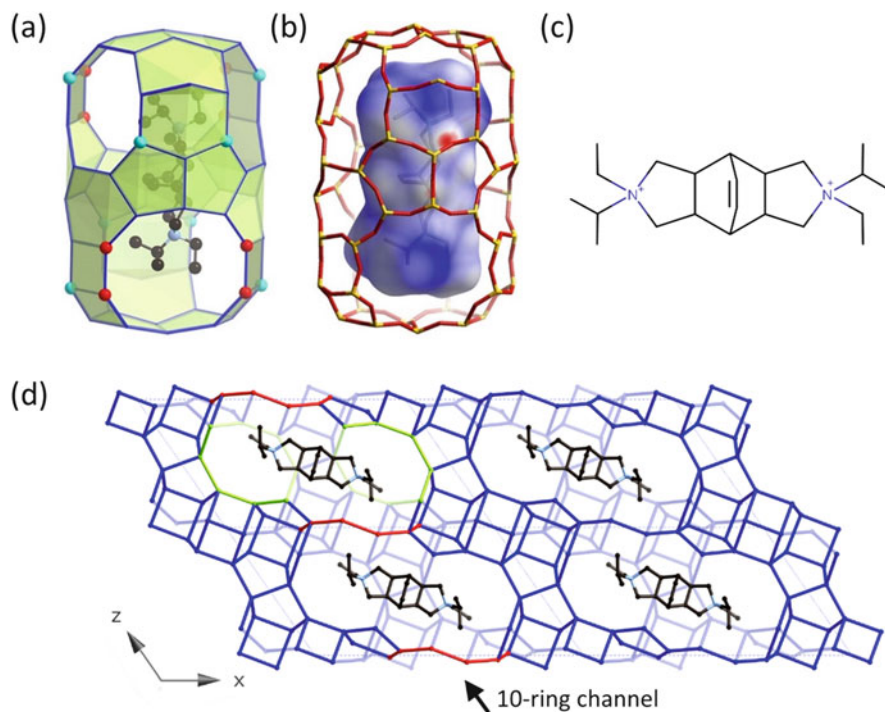


Fig. 8 Cavity of SSZ-87 showing (a) the refined position of the OSDA and the location of the two T-sites containing B in red and cyan, and (b) the Hirshfeld surface of the OSDA [87]. (c) Scheme of the OSDA. (d) Projection of the structure of SSZ-87 showing the arrangement of the large cavities and the position of the OSDA. Reprinted with permission from Ref. [78]. Copyright 2015 American Chemical Society

fourfold symmetry of the pore. Therefore, a model of the OSDA (Fig. 8c) was created and optimized using the energy minimization routine in Jmol [74]. It was not clear from the synthesis which configuration the OSDA would adopt, so XRD data on a single crystal of the OSDA were collected, revealing that the OSDA had twofold symmetry with the terminal isopropyl groups in a *cis* configuration. The OSDA was added to the structural model as a rigid-body, and its initial location and orientation were then optimized using simulated annealing. In this process, the OSDA settled on a position of fourfold disorder (point symmetry $2/m$). The twofold

rotation axis of the OSDA appeared to align itself with the twofold rotation axis of the framework, so the description of the OSDA was changed to align it with this axis, reducing the disorder by a factor of two. In the final stages of the refinement, the rigid-body description was replaced by a geometrically restrained one, and B could be located in the framework.

The refined structure reveals that the cavity wraps comfortably around the OSDA, with a minimum distance between the framework and the OSDA of 3.28 Å. All other distances are well over 3.6 Å. Interestingly, the two positively charged N atoms are located near the ends of the OSDA, close to the T-sites partially occupied by B (Fig. 8).

5.2 SSZ-61

Cell: $P2_1/c$, $a = 19.7601$ Å, $b = 10.0747$ Å, $c = 25.2192$ Å, $\beta = 106.92^\circ$
 Composition: $\text{IH}_4(\text{C}_{16}\text{H}_{26}\text{N})_4[\text{Si}_{80}\text{O}_{164}]$

SSZ-61 (*-SSO) is a high-silica zeolite with large one-dimensional, dumbbell-shaped 18-ring channels, and an interrupted framework structure that is closely related to that of **MTW** and **SFN** [79]. The location of the OSDA in this particular structure was not only determined from the powder diffraction data, it was used as an argument in the structure determination process. Structure analysis of SSZ-61 was initially attempted using a *C*-centred cell ($a = 19.76$ Å, $b = 5.04$ Å, $c = 25.22$ Å, $\beta = 106.9^\circ$), and resulted in only a partial structure. However, to accommodate the bulky OSDA (7.1 Å × 2.3 Å × 4.2 Å; Fig. 9b), the unit cell had to be doubled along *b*. The reasoning was that, in this way, two OSDA molecules could be arranged side by side, with their main axes parallel to the channel direction. With the expanded unit cell, the partial framework structure for SSZ-61 could be completed and confirmed against the XRPD data. However, the initial residual electron density map did not reveal any sign of the OSDA in the 18-ring pores, despite the fact that ^{13}C NMR clearly showed that the OSDA was intact (Fig. 9a). This could simply be an effect of the data quality, or problems with the estimation of the scale factor or background function. Therefore, an idealized model of the OSDA was constructed and added as a rigid-body. The initial location and orientation could then be found by applying the simulated annealing routine. This model was converted to a flexible model with geometric restraints for further refinement, which confirmed the framework structure and the location of the OSDA. In the refined structure, each half of the 18-ring channel in SSZ-61 accommodates one OSDA cation to give a total of four per unit cell (Fig. 9c, d). The dumbbell-shaped pore provides room for the bulky part of the OSDA, and allows the positively charged N atom to lie near two terminal O atoms.

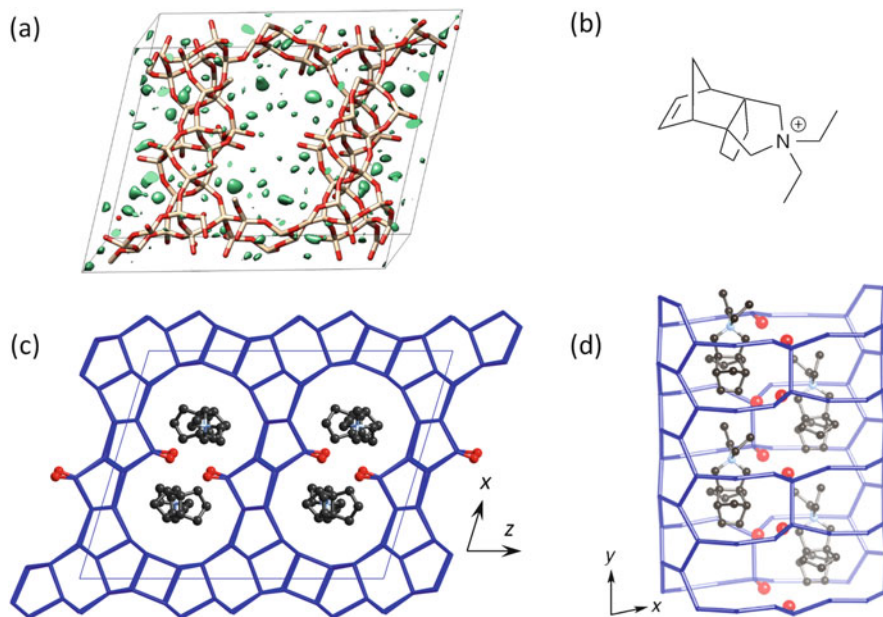


Fig. 9 (a) Initial difference electron density map calculated with only the framework structure of SSZ-61 along the channel direction. (b) Scheme of the OSDA. Framework structure of SSZ-61 showing the 18-ring channels and the location of the OSDAs viewed (c) down the channel and (d) from the side. The terminal O atoms are shown in red and other O and H atoms have been omitted for clarity

5.3 DAF-1

Cell: $P6/mmc$, $a = 22.2244 \text{ \AA}$, $b = 42.3293 \text{ \AA}$

Composition: $[(C_9H_{17}N_2)_{17.2}F_4(H_2O, OH, F)_{29.8}][Zn_{6.1}Al_{125.9}P_{132}O_{528}]$

In a study exploring the use of ionic liquid reactions based on imidazolium halides, Pinar et al. found a new zincoaluminophosphate zeolite with the **DFO** framework type that they termed Zn-DAF-1 [43]. **DFO** has an open framework structure with a three-dimensional channel system consisting of two separate parallel 12-ring channels along the c -axis, linked via perpendicular 10- and 8-ring channels. With the goal of locating the Zn in the framework and the N,N' -di-isopropyl-imidazolium (DIPI) ions (Fig. 10c) in the pores, a full structure analysis was performed. Rietveld refinement was initiated using the published coordinates for Mg-DAF-1, and after a scale factor had been estimated using the steps described in Sect. 4, a difference map was generated. Pinar et al. write that although the difference map revealed a few small clouds of electron density in the void volume of the structure (Fig. 10a, b), the high symmetry of the framework made it difficult to interpret these clouds. Therefore, they made an educated guess for the approximate positions of the OSDA. Although these four positions were not necessarily accurate, it did improve the structural model so that

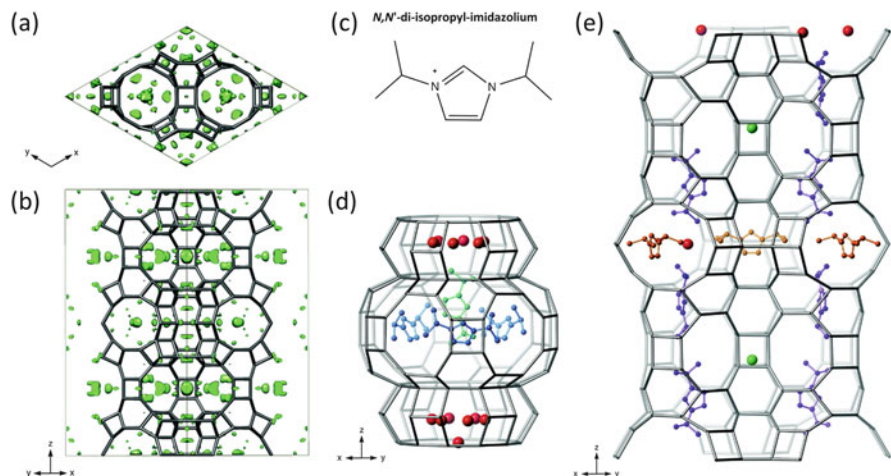


Fig. 10 Initial difference electron density map calculated with only the framework structure of DAF-1 along (a) the [001] and (b) [110] directions. (c) Scheme of the OSDA. Possible arrangements of (d) DIPI-1 (blue) and DIPI-2 (green) in the large cavity and the water molecules in the smaller cavity (red balls), and (e) DIPI-3 (purple), DIPI-4 (orange), the fluoride ions (green balls), and the water molecules (red balls). Framework oxygen atoms have been omitted for clarity. Reproduced from Ref. [43] with permission from the Centre National de la Recherche Scientifique (CNRS) and The Royal Society of Chemistry

the scale factor could be refined and the Zn atoms located. The four crystallographically independent sites (two per 12-ring channel) that could host the OSDA were found, but attempts to refine the atomic positions failed, even with strong geometric restraints. In the end, a model with hard constraints to keep the imidazolium rings planar, and the isopropyl moieties chemically sensible, led to a better positioning of the OSDA species and a cleaner final difference map (Fig. 10d, e). H atoms on the OSDAs were taken into account by increasing the population factors of the C atoms, and the occupancy of each OSDA was refined, giving a total of 17.2 OSDA atoms in the 22 positions available per unit cell. The authors comment that this model yielded a reasonable geometry and a good profile fit.

This study is interesting, because the position of four crystallographically independent OSDAs could be determined from XRPD data, and highlights the necessity for a careful, systematic approach to structure refinement. The main difficulty was that the DIPI does not follow the high symmetry of the framework and is therefore disordered. For example, one of the OSDA atoms lies close to the special position where the sixfold rotation axis and the mirror plane perpendicular to it intersect. It is therefore disordered over 12 equivalent positions, but only one of these 12 positions is occupied at a time. This not only makes it difficult to interpret the shape of the density cloud, but also dilutes its intensity by a factor 12. Another OSDA is located on a similar symmetry element, but there three out of 12 positions can be occupied simultaneously. It is worth noting that locating four OSDAs using simulated annealing would therefore be problematic.

5.4 SSZ-74

Cell: Cc , $a = 20.4756 \text{ \AA}$, $b = 13.3839 \text{ \AA}$, $c = 20.0859 \text{ \AA}$, $\beta = 102.1^\circ$

Composition: $[\text{C}_{16}\text{H}_{34}\text{N}_2]_4[\text{Si}_{92}\text{O}_{184}(\text{OH})_8]$

SSZ-74 (-SVR) is a high-silica zeolite catalyst with a 3-dimensional 10-ring channel system, and ordered Si vacancies [80]. Structure analysis was performed using high-resolution powder diffraction data, collected on the as-synthesized material, because significant line broadening had been observed upon the removal of the OSDA. Although difference Fourier maps showed a cloud of electron density in the pores, the individual atoms of the 1,6-(*N*-methylpyrrolidinium)-hexane (Fig. 11d) used to synthesize the material could not be resolved. Therefore molecular modelling was used to estimate the positions using the energy-optimization docking procedure described by Burton et al. [81]. Rietveld refinement was started using this as the initial position of the OSDA, with geometric restraints imposed on the bond distances and angles of both the framework and the OSDA. The final refinement showed the OSDA taking its place in the centre of the large cavity (Fig. 11a), with the two closest contacts between the terminal oxygen atoms at the Si vacancy to the two nitrogen atoms of the doubly charged OSDA at 3.62 \AA ($\text{O}33 \cdots \text{N}5$) and 3.58 \AA ($\text{O}3 \cdots \text{N}13$).

The position found at the end of the refinement deviates significantly from the one determined initially with molecular modelling (Fig. 11b, c), perhaps because it was not known when the molecular modelling was performed that there was a Si vacancy in the framework. This example nicely highlights the potential of combining molecular modelling with Rietveld refinement and the fact that refinement can indeed correct deficiencies in the initial model.

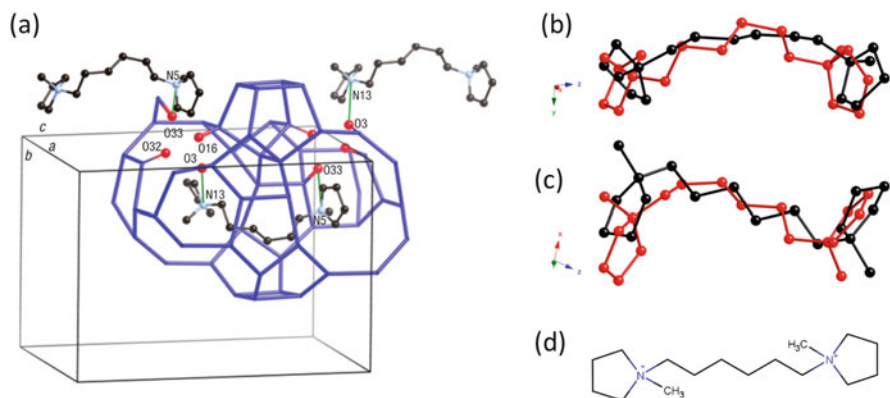


Fig. 11 (a) A portion of the structure of SSZ-74 showing the position of the OSDA. (b) Conformations of the OSDA found using molecular modelling assuming a fully connected framework structure in *black* and from the final refinement in *red*, and (c) the same projection rotated by 90° . (d) Scheme of the OSDA

5.5 RUB-50

Cell: $R\bar{3}m$, $a = 13.1090 \text{ \AA}$, $c = 22.4740 \text{ \AA}$

Composition: $[\text{Na}_{0.24}\text{H}_{4.9}(\text{C}_6\text{H}_{17}\text{NO})_{5.8}][\text{Si}_{48.86}\text{Al}_{5.14}\text{O}_{108}]$

RUB-50 is an aluminosilicate zeolite with a two-dimensional 8-ring channel system that can be synthesized using diethyldimethylammonium (DEDMA; Fig. 12d) as the OSDA. It has a LEV-type framework structure, which can be described as an AABCCABBC sequence of 6-ring layers (it is a member of the ABC-6 family of framework structures). As part of a study into the physicochemical properties of RUB-50, Yamamoto et al. performed a structure refinement of as-synthesized RUB-50 using lab XRPD data [82]. The refinement was initiated using the LEV framework model. The OSDA was approximated using a dummy atom with the scattering amplitude of $\text{C}_6\text{H}_{16}\text{N}$, and then Na^+ could be located in the difference map (Fig. 12a). Although the refinement converged, and resulted in a good fit to the data, the authors did not leave it at that. The disordered arrangement of the OSDA in the *lev* cavity was found from the electron density distribution determined using the maximum entropy method (MEM) [83] with the program PRIMA (now Dynomia) [84]. MEM is itself model free and only structure factors from isolated (non-overlapping) reflections were used for the analysis. After the initial MEM analysis, the electron density distribution was redetermined using MEM-based pattern fitting (MFP), which combines MEM analysis and whole-pattern fitting, making it efficient in representing highly disordered atomic arrangements. In this way, the position of the disordered OSDA, OH^- , and water molecules could be found (Fig. 12b). Their results suggest that the electron density distribution of the OSDA is anisotropically elongated to form a “garlic” shape (Fig. 12b). Yamamoto et al. note that this is probably because the OSDA is disordered around the threefold axis and because hydroxyl ions or water molecules are close to the OSDA. These findings were then fed back into the Rietveld refinement to confirm that the location of the OSDA is sensible.

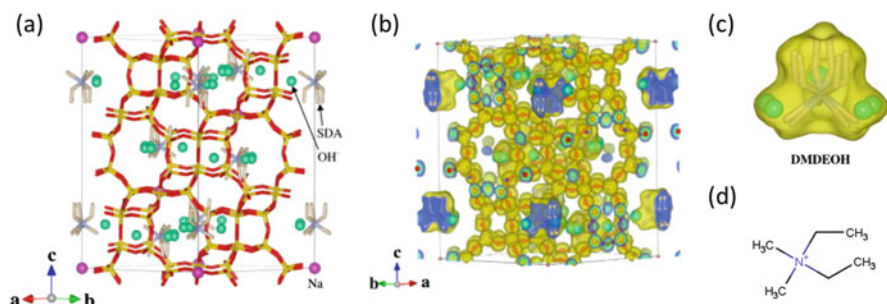


Fig. 12 (a) Structure of the as-made RUB-50 obtained from the Rietveld refinement, and electron density maps of (b) the structure and (c) the disordered OSDA, both obtained using MFP refinement. (d) Scheme of the OSDA. Reprinted from Ref. [82] with permission from Elsevier

5.6 STA-2

Cell: $R\bar{3}$, $a = 12.726 \text{ \AA}$, $c = 30.939 \text{ \AA}$

Composition: $(\text{BDAB})_3[\text{Al}_{12}\text{P}_{12}\text{O}_{24}]$, $\text{BDAB} = \text{C}_{18}\text{H}_{32}\text{N}_2$

The aluminophosphate zeolite STA-2 (SAT) was initially prepared and characterized by Noble et al. in 1997 using 1,4-bis-*N*-quinuclidiniumbutane (BQNB; Fig. 13c) as the OSDA [85]. Its framework structure could be determined using synchrotron microcrystal XRD, and was found to be a member of the ABC-6 family with an ABBCBCCACAAB stacking sequence of 6-ring layers, giving it a three-dimensional 8-ring channel system. All atoms of the OSDA could be located from the difference map, confirming its location along the threefold axis (Fig. 13a). The authors note that although there is a disorder in the positions of the atoms within the tetramethylene chain, as seen in the larger temperature factors and chemically inaccurate bond lengths for C–N and C–C, the positions of the quinuclidinium fragments are particularly well described. This is probably because the quinuclidinium fragments have a threefold axis that can line up with that of the framework, so only the atoms in the connecting methylene chain are disordered.

A follow-up study appeared in 2010, with the aim of finding a cheaper OSDA to produce STA-2. To do this, Castro et al. investigated a series DABCO-derived OSDAs (DABCO = diazabicyclooctane) using molecular modelling, and found bis-diazabicyclooctane-butane (BDAB; Fig. 13d) to give the lowest framework stabilization energy (Fig. 13b) [86]. This is not surprising, because BDAB is essentially identical to BQNB, with the exception that two tertiary C atoms at either end are replaced by two tertiary amine N atoms. They were able to produce

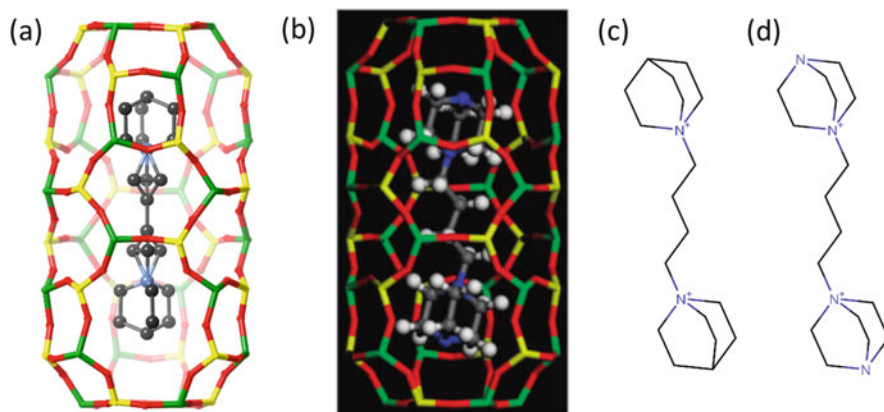


Fig. 13 SAT-cage including the position of the OSDA as determined using (a) microcrystal diffraction data and (b) molecular modelling. Scheme of (c) 1,4-bis-*N*-quinuclidiniumbutane (BQNB) and (d) bis-diazabicyclooctane-butane (BDAB), representing the OSDAs in (a) and (b), respectively. (a) Reprinted (adapted) with permission from [86]. Copyright 2010 American Chemical Society

STA-2 using BDAB as the OSDA, and performed a Rietveld refinement with the XRPD data to confirm the structure of STA-2.

6 Discussion/Conclusion

From our work on as-synthesized zeolites, we find that the OSDA is often highly ordered, despite the fact that their locations usually have to be described as a superposition of multiple discrete positions. Indeed, they probably do occupy each of these symmetry-related positions in different unit cells in the crystal. The OSDA just does not have the fully symmetry of the zeolite framework structure, and therefore appears to be more disordered than it is. The examples presented in this chapter demonstrate that given enough attention, the OSDA can be located systematically using diffraction methods. Difficulties in locating the OSDA can often be attributed to the lack of high-quality data, in particular when working with XRPD data, for which reflection overlap obfuscates the true reflection intensities. Part of the information that is lost can be overcome by using modern approaches like simulated annealing and/or by using supplementary information gained from other measurements. MAS NMR is particularly useful in determining whether the OSDA is intact and/or protonated.

The reliability of the structure analysis will also depend upon the specific problem at hand. For example, a rigid OSDA will generally be easier to locate than a flexible one, an OSDA with at least a subset of the symmetry of the framework will be easier to refine than one with no symmetry relationship, and an OSDA at a position of low symmetry will be easier to locate and recognize than one near a symmetry element.

Despite the constant improvement in the quality of diffraction data, and structure determination and refinement techniques, locating an OSDA from diffraction data cannot yet be taken for granted. We hope that some of the information provided here will provide the reader with some insight into how the problem can be approached in a systematic manner and where some of the pitfalls lie.

Acknowledgements S.S. thanks the Swiss National Science Foundation for financial support (project number: 165282) and L.M. Chevron ETC.

References

1. Barrer RM, Denny PJ (1961) *J Chem Soc* 971–982. doi:10.1039/JR9610000971
2. Lok BM, Cannan TR, Messina CA (1983) *Zeolites* 3(4):282–291
3. Lobo RF, Zones SI, Davis ME (1995) *J Incl Phenom Macrocycl Chem* 21(1–4):47–78
4. Gies H, Marler B (1992) *Zeolites* 12(1):42–49
5. Gies H (1994) In: Jansen JC, Stöcker M, Karge HG, Weitkamp J (eds) *Advanced zeolite science and applications*, vol 85, Elsevier, pp 295–327

6. Kubota Y, Helmkamp MM, Zones SI, Davis ME (1996) *Microporous Mater* 6(4):213–229
7. Millini R, Carluccio L, Frigerio F, O'Neil Parker W, Bellussi G (1998) *Micropor Mesopor Mat* 24(4–6):199–211
8. Wagner P, Nakagawa Y, Lee GS, Davis ME, Elomari S, Medrud RC, Zones SI (2000) *J Am Chem Soc* 122(2):263–273
9. McCusker LB, Baerlocher C (in press) In: Vol H, Gilmore CJ, Kaduk J, Schenk H (eds) *International tables for crystallography*, Wiley
10. Baerlocher C, McCusker LB. Database for zeolite structures. <http://www.iza-structure.org/databases/>
11. Jordá JL, Rey F, Sastre G, Valencia S, Palomino M, Corma A, Segura A, Errandonea D, Lacomba R, Manjón FJ, Gomis Ó, Kleppe AK, Jephcoat AP, Amboage M, Rodríguez-Velamazán JA (2013) *Angew Chem* 125(40):10652–10656
12. Roth WJ, Nachtigall P, Morris RE, Wheatley PS, Seymour VR, Ashbrook SE, Chlubná P, Grajciar L, Položij M, Zukal A, Shvets O, Čejka J (2013) *Nat Chem* 5(7):628–633
13. Chlubná-Eliášová P, Tian Y, Pinar AB, Kubr UM, Čejka J, Morris RE (2014) *Angew Chem* 126(27):7168–7172
14. Breck DW, Eversole WG, Milton RM, Reed TB, Thomas TL (1956) *J Am Chem Soc* 78(23):5963–5972
15. Reed TB, Breck DW (1956) *J Am Chem Soc* 78(23):5972–5977
16. Gramlich V, Meier WM (1971) *Z Kristallografiya* 133(1–6):134–149
17. Baerlocher C, Meier WM (1969) *Helv Chim Acta* 52(7):1853–1860
18. Baerlocher C, Meier WM (1970) *Helv Chim Acta* 53(6):1285–1293
19. Argauer RJ, Landolt GR (1972) Crystalline zeolite ZSM-5 and method of preparing the same. US3702886 A
20. Flanigen EM, Bennett JM, Grose RW, Cohen JP, Patton RL, Kirchner RM, Smith JV (1978) *Nature* 271(5645):512–516
21. Kokotailo GT, Lawton SL, Olson DH, Meier WM (1978) *Nature* 272(5652):437–438
22. Price GD, Pluth JJ, Smith JV, Araki T, Bennett JM (1981) *Nature* 292(5826):818–819
23. Baerlocher C (1984) In: Olson DH, Bisio A (eds) 6th Int Zeolite Conf.; Guildford Butterworths: Reno, pp 823–833
24. van Koningsveld H, van Bekkum H, Jansen JC (1987) *Acta Cryst B* 43(2):127–132
25. Bennett JM, Cohen JP, Flanigen EM, Pluth JJ, Smith JV (1983) In: *Intrazeolite chemistry*, ACS Symposium Series, vol 218, American Chemical Society, pp 109–118
26. Parise JB (1984) *J Chem Soc Chem Commun* 21:1449–1450
27. Parise JB (1984) *Acta Crystallogr C* 40(10):1641–1643
28. Gies H (1983) *Z Kristallogr* 164(3–4):247–257
29. Gerke H, Gies H (1984) *Z Kristallogr* 166(1–4):11–22
30. Gies H (1984) *Z Kristallogr* 167(1–4):73–82
31. Gies H (1986) *Z Kristallogr* 175(1–4):93–104
32. McCusker L (1988) *J Appl Cryst* 21(4):305–310
33. Harrison WTA, Martin TE, Gier TE, Stucky GD (1992) *J Mater Chem* 2(2):175–181
34. Harrison WTA, Nenoff TM, Eddy MM, Martin TE, Stucky GD (1992) *J Mater Chem* 2(11):1127–1134
35. Parise JB (1986) *Acta Cryst C* 42(6):670–673
36. Loiseau T, Férey G (1992) *J Chem Soc Chem Commun* 17:1197–1198
37. Weigel SJ, Morris RE, Stucky GD, Cheetham AK (1998) *J Mater Chem* 8(7):1607–1611
38. Wragg DS, Bull I, Hix GB, Morris RE (1999) *Chem Commun* 20:2037–2038
39. Davis ME, Saldarriaga C, Montes C, Garces J, Crowder C (1988) *Zeolites* 8(5):362–366
40. Richardson JW, Smith JV, Pluth JJ (1989) *J Phys Chem* 93(25):8212–8219
41. McCusker LB, Baerlocher C, Jahn E, Bülow M (1991) *Zeolites* 11(4):308–313
42. Pinar AB, McCusker LB, Baerlocher C, Schmidt J, Hwang S-J, Davis ME, Zones SI (2015) *Dalton Trans* 44(13):6288–6295

43. Pinar AB, McCusker LB, Baerlocher C, Hwang S-J, Xie D, Benin AI, Zones SI (2016) *New J Chem* 40(5):4160–4166
44. Bergmann J, Le Bail A, Shirley R, Zlokazov V (2004) *Z Kristallogr Cryst Mater* 219(12):783–790
45. Rietveld HM (1969) *J Appl Cryst* 2(2):65–71
46. Giacobozzo C, Monaco HL, Artioli G, Viterbo D, Ferraris G, Gilli G, Zanotti G, Catti M (2002) *Fundamentals of crystallography*. In: Giacobozzo C Series Ed., Oxford Science Publications
47. McCusker LB, Von Dreele RB, Cox DE, Louër D, Scardi P (1999) *J Appl Crystallogr* 32(1):36–50
48. Young RA (1993) *The rietveld method*. In: Young RA, Series Ed, Oxford University Press
49. Coelho AA (2012) TOPAS-ACADEMIC v5.0
50. Toby BH, Von Dreele RB (2013) *J Appl Crystallogr* 46(2):544–549
51. Rodríguez-Carvajal J (1990) In: Galy J, Louër D (eds) *Abstracts of the meeting on powder diffraction (Toulouse, France)*, pp 127–128
52. Le Bail A, Duroy H, Fourquet JL (1988) *Mater Res Bull* 23(3):447–452
53. Pawley GS (1981) *J Appl Crystallogr* 14(6):357–361
54. Baerlocher C, Hepp A, Meier WM (1976) DLS-76
55. Gale JD, Rohl AL (2003) *Mol Simul* 29(5):291–341
56. Momma K, Izumi F (2011) *J Appl Crystallogr* 44(6):1272–1276
57. Pettersen EF, Goddard TD, Huang CC, Couch GS, Greenblatt DM, Meng EC, Ferrin TE (2004) *J Comput Chem* 25(13):1605–1612
58. Smeets S, McCusker LB, Baerlocher C, Elomari S, Xie D, Zones SI (2016) *J Am Chem Soc* 138(22):7099–7106
59. David WIF, Shankland K (2008) *Acta Cryst A* 64(1):52–64
60. Deem MW, Newsam JM (1989) *Nature* 342(6247):260–262
61. Porcher F, Borissenko E, Souhassou M, Takata M, Kato K, Rodríguez-Carvajal J, Lecomte C (2008) *Acta Crystallogr B* 64(6):713–724
62. Fyfe CA, Lee JSJ, Cranswick LMD, Swainson I (2008) *Micropor Mesopor Mat* 112(1–3):299–307
63. Meilikhov M, Yusenko K, Fischer RA (2010) *Dalton Trans* 39(45):10990–10999
64. Dejoie C, Martinetto P, Tamura N, Kunz M, Porcher F, Bordat P, Brown R, Dooryhée E, Anne M, McCusker LB (2014) *J Phys Chem C* 118(48):28032–28042
65. Inge AK, Huang S, Chen H, Moraga F, Sun J, Zou X (2012) *Cryst Growth Des* 12(10):4853–4860
66. Xu Y, Liu L, Chevrier DM, Sun J, Zhang P, Yu J (2013) *Inorg Chem* 52(18):10238–10244
67. Chen R, Yao J, Gu Q, Smeets S, Baerlocher C, Gu H, Zhu D, Morris W, Yaghi OM, Wang H (2013) *Chem Commun* 49(82):9500–9502
68. Reimer N, Reinsch H, Inge AK, Stock N (2015) *Inorg Chem* 54(2):492–501
69. Halis S, Inge AK, Dehning N, Weyrich T, Reinsch H, Stock N (2016) *Inorg Chem* 55(15):7425–7431
70. Favre-Nicolin V, Černý R (2002) *J Appl Crystallogr* 35(6):734–743
71. David WIF, Shankland K, van de Streek J, Pidcock E, Motherwell WDS, Cole JC (2006) *J Appl Crystallogr* 39(6):910–915
72. Allen FH (2002) *Acta Crystallogr B* 58(3):380–388
73. Hanwell MD, Curtis DE, Lonie DC, Vandermeersch T, Zurek E, Hutchison GR (2012) *J ChemInform* 4(1):17–17
74. Hanson RM (2010) *J Appl Cryst* 43(5):1250–1260
75. Weininger D (1988) *J Chem Inf Comput Sci* 28(1):31–36
76. O’Boyle NM, Banck M, James CA, Morley C, Vandermeersch T, Hutchison GR (2011) *J Chem* 3(1):33
77. Prince E (ed) (2006) *International tables for crystallography: mathematical, physical and chemical tables, vol C, 1st edn*. Fuess H, Hahn T, Wondratschek H, Müller U, Shmueli U,

- Prince E, Authier A, Kopský V, Litvin DB, Rossmann MG, Arnold E, Hall S, McMahon B, Series Eds, International tables for crystallography; International Union of Crystallography, Chester, England
78. Smeets S, McCusker LB, Baerlocher C, Xie D, Chen C-Y, Zones SI (2015) *J Am Chem Soc* 137(5):2015–2020
79. Smeets S, Xie D, Baerlocher C, McCusker LB, Wan W, Zou X, Zones SI (2014) *Angew Chem* 126(39):10566–10570
80. Baerlocher C, Xie D, McCusker LB, Hwang S-J, Chan IY, Ong K, Burton AW, Zones SI (2008) *Nat Mater* 7(8):631–635
81. Burton A, Lee GS, Zones SI (2006) *Micropor Mesopor Mat* 90(1–3):129–144
82. Yamamoto K, Ikeda T, Onodera M, Muramatsu A, Mizukami F, Wang Y, Gies H (2010) *Micropor Mesopor Mat* 128(1–3):150–157
83. Collins DM (1982) *Nature* 298(5869):49–51
84. Momma K, Ikeda T, Belik AA, Izumi F (2013) *Powder Diffract* 28(3):184–193
85. Noble GW, Wright PA, Kvick Å (1997) *Dalton Trans* (23):4485–4490
86. Castro M, Seymour VR, Carnevale D, Griffin JM, Ashbrook SE, Wright PA, Apperley DC, Parker JE, Thompson SP, Fecant A, Bats N (2010) *J Phys Chem C* 114(29):12698–12710
87. Spackman MA, Jayatilaka D (2009) *CrstEngComm* 11(1):19–32
88. Cambor MA, Díaz-Cabañas M-J, Perez-Pariente J, Teat SJ, Clegg W, Shannon IJ, Lightfoot P, Wright PA, Morris RE (1998) *Angew Chem Int Ed* 37(15):2122–2126
89. Bu X, Feng P, Gier TE, Zhao D, Stucky GD (1998) *J Am Chem Soc* 120(51):13389–13397
90. Bu X, Feng P, Stucky GD (1998) *J Am Chem Soc* 120(43):11204–11205
91. Josien L, Simon A, Gramlich V, Patarin J (2001) *Chem Mater* 13(4):1305–1311
92. Ove Kongshaug K, Fjellvåg H, Petter Lillerud K (2001) *J Mater Chem* 11(4):1242–1247
93. Marler B, Werthmann U, Gies H (2001) *Micropor Mesopor Mat* 43(3):329–340
94. Wheatley PS, Morris RE (2002) *J Solid State Chem* 167(2):267–273
95. Jordá JL, McCusker LB, Baerlocher C, Morais CM, Rocha J, Fernandez C, Borges C, Lourenco JP, Ribeiro MF, Gabelica Z (2003) *Micropor Mesopor Mat* 65(1):43–57
96. Yang X, Cambor MA, Lee Y, Liu H, Olson DH (2004) *J Am Chem Soc* 126(33):10403–10409
97. Zanardi S, Alberti A, Cruciani G, Corma A, Fornés V, Brunelli M (2004) *Angew Chem Int Ed* 43(37):4933–4937
98. Li Y, Zou X (2005) *Angew Chem Int Ed* 44(13):2012–2015
99. Parnham ER, Morris RE (2006) *Chem Mater* 18(20):4882–4887
100. Tang L, Shi L, Bonneau C, Sun J, Yue H, Ojuva A, Lee B-L, Kritikos M, Bell RG, Bacsik Z, Mink J, Zou X (2008) *Nat Mater* 7(5):381–385
101. Su J, Wang Y, Wang Z, Lin J (2009) *J Am Chem Soc* 131(17):6080–6081
102. Armstrong JA, Weller MT (2010) *J Am Chem Soc* 132(44):15679–15686
103. Broach RW, Kirchner RM (2011) *Micropor Mesopor Mat* 143(2–3):398–400
104. Liu Z, Song X, Li J, Li Y, Yu J, Xu R (2012) *Inorg Chem* 51(3):1969–1974
105. Shao L, Li Y, Yu J, Xu R (2012) *Inorg Chem* 51(1):225–229
106. Xie D, McCusker LB, Baerlocher C, Zones SI, Wan W, Zou X (2013) *J Am Chem Soc* 135(28):10519–10524
107. Wang Y, Li Y, Yan Y, Xu J, Guan B, Wang Q, Li J, Yu J (2013) *Chem Commun* 49(79):9006–9008
108. Broach RW, Greenlay N, Jakubczak P, Knight LM, Miller SR, Mowat JPS, Stanczyk J, Lewis GJ (2014) *Micropor Mesopor Mat* 189:49–63
109. Smeets S, Xie D, McCusker LB, Baerlocher C, Zones SI, Thompson JA, Lacheen HS, Huang H-M (2014) *Chem Mater* 26(13):3909–3913
110. Willhammar T, Burton AW, Yun Y, Sun J, Afeworki M, Strohmaier KG, Vroman H, Zou X (2014) *J Am Chem Soc* 136(39):13570–13573
111. Smeets S, Koch L, Mascello N, Sesseg J, Hernández-Rodríguez M, Mitchell S, Pérez-Ramírez J (2015) *CrstEngComm* 17(26):4865–4870

Location of OSDAs in Zeolites Using Diffraction Techniques

112. Bae J, Cho J, Lee JH, Seo SM, Hong SB (2016) *Angew Chem* 128(26):7495–7499
113. Kang JH, Xie D, Zones SI, Smeets S, McCusker LB, Davis ME (2016) *Chem Mater* 28(17):6250–6259
114. Guo P, Strohmaier K, Vroman H, Afeworki M, Ravikovitch PI, Paur CS, Sun J, Burton A, Zou X (2016) *Inorg Chem Front* 3(11):1444–1448
115. Chen F-J, Gao Z-H, Liang L-L, Zhang J, Du H-B (2016) *CrstEngComm* 18(15):2735–2741